Electronic Supplementary Material (ESI) for Journal of Materials Chemistry C.

Facile synthesis of ultralight S-doped Co_3O_4 microflowers@reduced graphene oxide aerogel with defect and interface engineering for broadband electromagnetic wave absorption

Hui Gao, Shougang Chen, Shuang Wei, Wen Li, Mutian Zhang, Ning Sun*

School of Materials Science and Engineering, Ocean University of China, Qingdao 266100, China

E-mail: sgchen@ouc.edu.cn

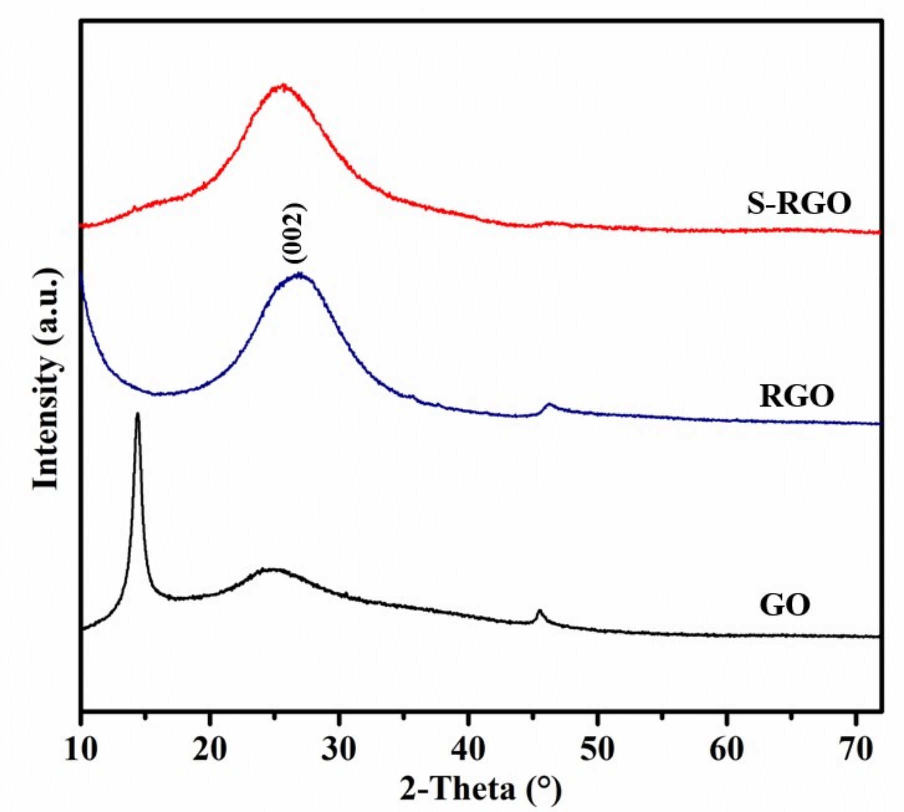

Fig. S1. XRD patterns of GO, RGO and S-RGO.

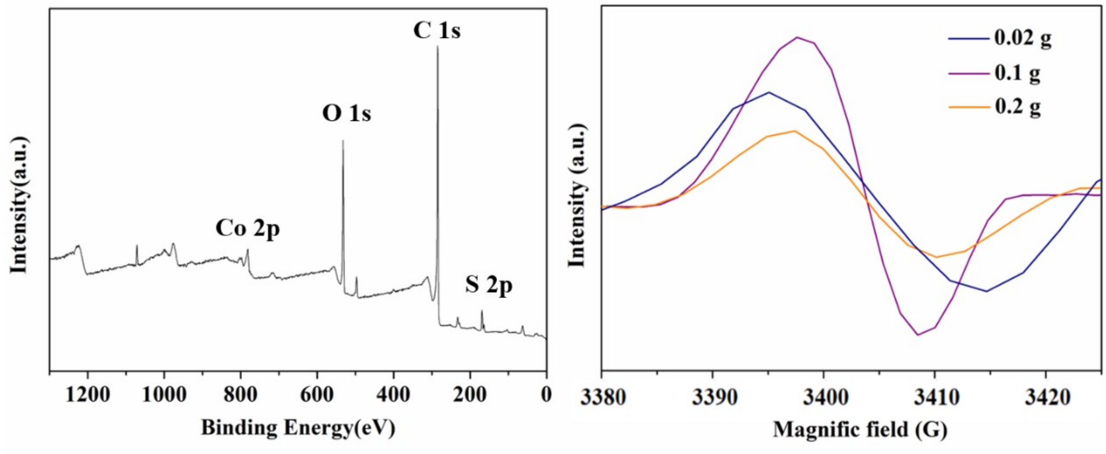

Fig. S2. (a) The survey scan spectrum of S-Co_3O_4@RGO aerogel, (b) EPR spctra of S-Co_3O_4@RGO-2, S-Co_3O_4@RGO-10 and S-Co_3O_4@RGO-20.

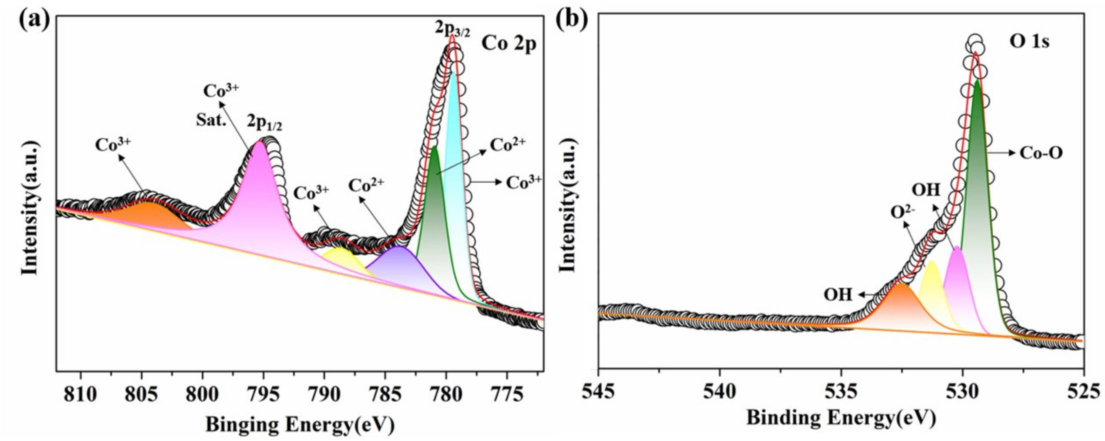

Fig. S3. XPS analysis of Co_3O_4: (a) Co 2p, (b) O 1s.

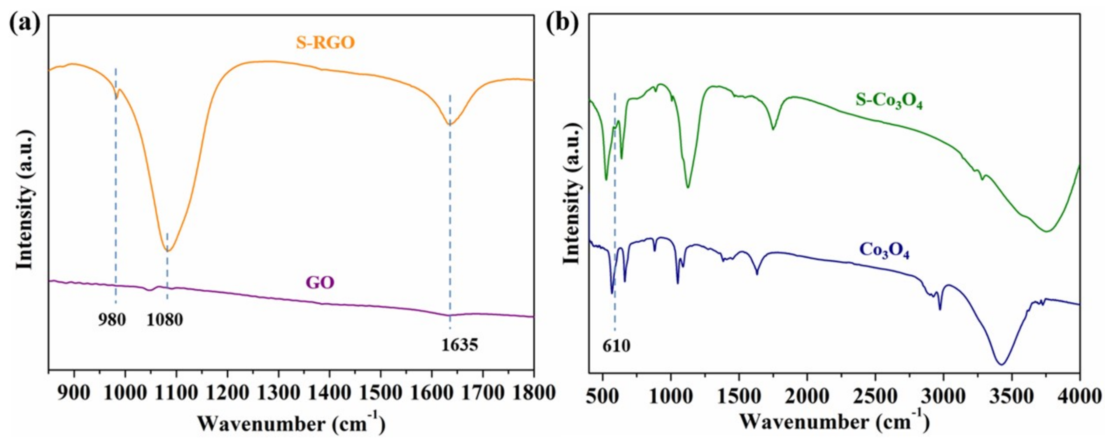

Fig. S4. FTIR spectra of (a) GO and S-RGO, (b) Co_3O_4 and S-Co_3O_4.

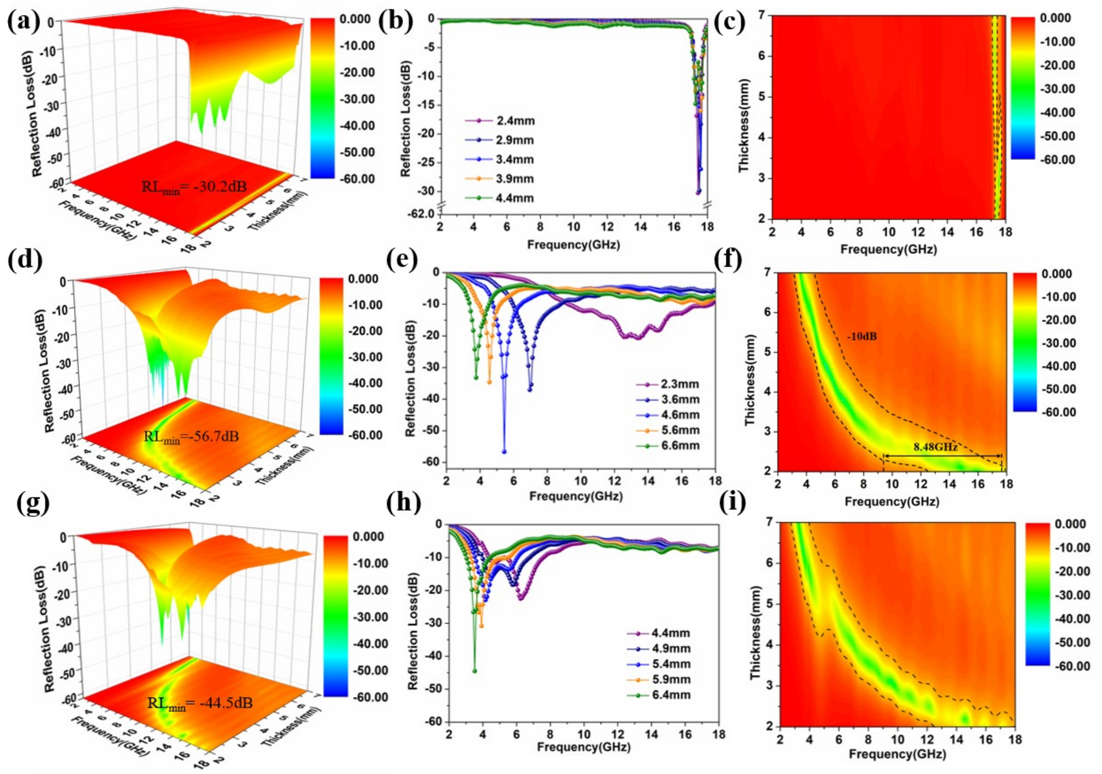

Fig. S5. 3D RL projection mappings, RL curves with different thickness and 2D RL contour maps of (a-c) S-Co_3O_4@RGO-2, (d-f) S-Co_3O_4@RGO-10, (g-i) S-Co_3O_4@RGO-20 with filling ratio of 5 wt.%.

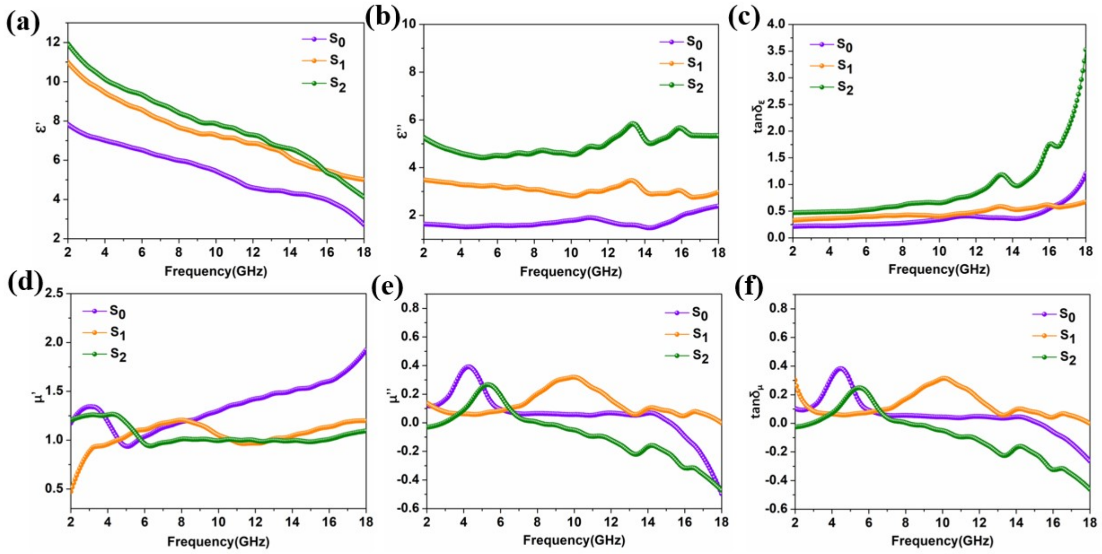

Fig. S6. (a, b) the ε' and ε'' of complex permittivity, (c) $tan\delta_{\varepsilon}$, (d, e) the μ' and μ'' of the complex permeability, (f) $tan\delta_{\mu}$ of S_0, S_1 and S_2.

To further investigate the effect of Co_3O_4 and RGO ratios on the EMA properties, three types of 3D S-Co_3O_4/RGO aerogels with different mass ratios of Co_3O_4 and RGO (2:1, 1:1, 1:2) are prepared, marked as S_0, S_1 and S_2, respectively. As displayed in Fig. S6a-S6f, the ε' values of S_0, S_1 and S_2 decrease from 7.8 to 2.7, 11.1 to 5.3 and 12.0 to 4.2, respectively, while the ε'' values of S_0, S_1 and S_2 maintain at 1.8, 3 and 5 in 2.0-18.0 GHz, respectively. With the increase of RGO mass fraction in the S-Co_3O_4@RGO composite, both the ε' and ε'' values increase, which indicates the enhanced conduction loss and polarization relaxation. However, too excessive dielectric loss brings the mismatching between ε_r and μ_r. Then, EMW cannot enter the absorber, which is not favourable to the EMA. The RL_{min} value of S_0 is -42.1 dB at 2.0 mm (Fig. S7a-S7c). As presented in Fig. S7d-S7f, the RL_{min} value of S_1 can reach up to -56.7 dB at 5.44 GHz with the matching thickness of 3.6 mm. The RL_{min} value of S_2 is -26.6 dB at 7.0 mm (Fig. S7g-S7i). From above discussion, the EMA performance of the S_1 sample is optimal. The 1:1 ratio of RGO/Co_3O_4 endows the appropriate balance between good impedance matching and strong loss capability.

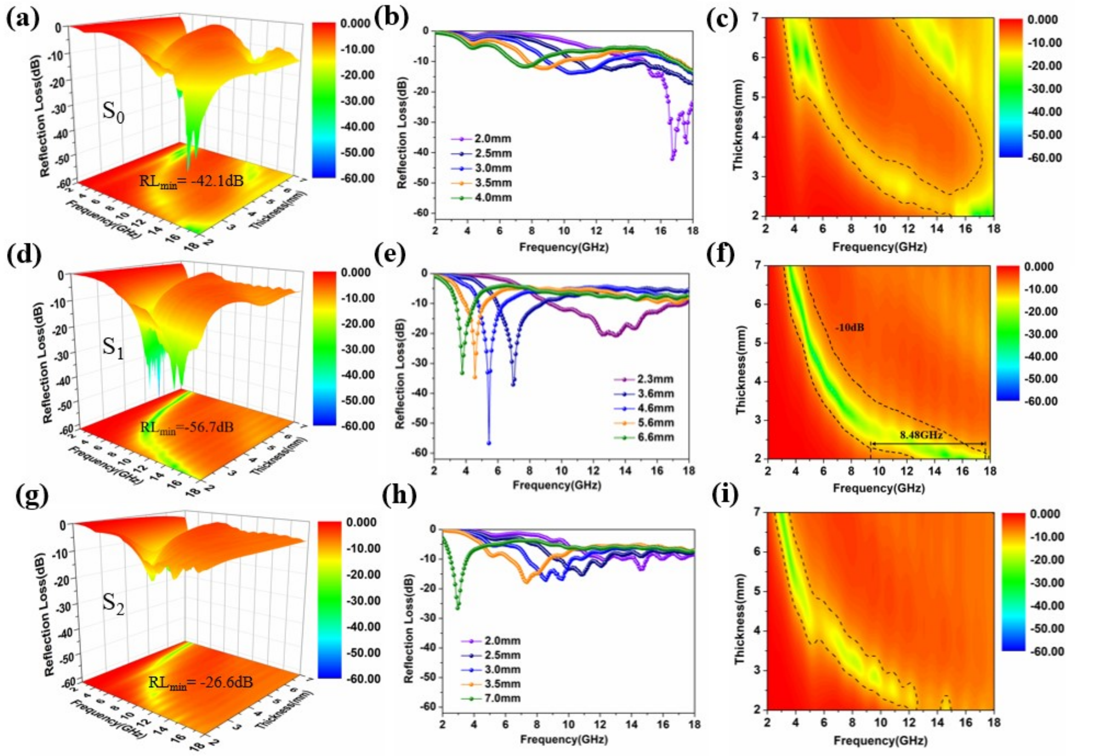

Fig. S7. 3D RL projection mappings, RL curves with different thickness and 2D RL contour maps of (a-c) S_0, (d-f) S_1, (g-i) S_2 with filling ratio of 5 wt.%.

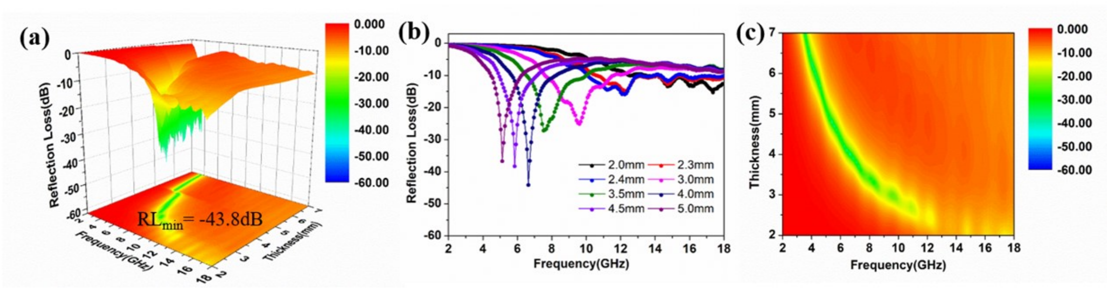

Fig. S8. (a) 3D RL projection mappings, (b) RL curves with different thickness and (c) 2D RL contour maps of R_2 under 10 wt.% loading.

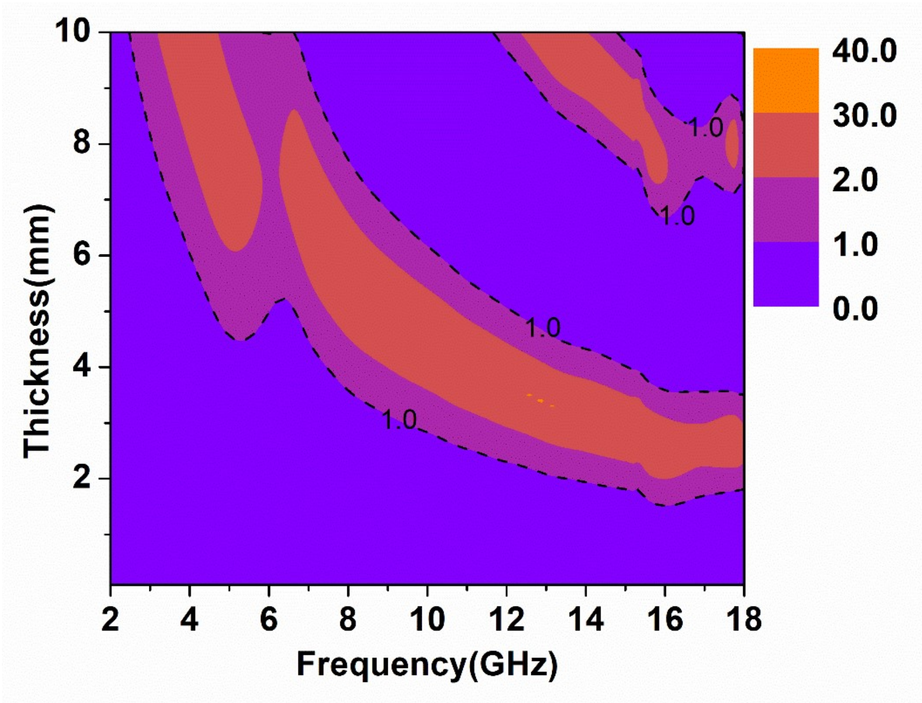

Fig. S9. Two-dimensional contour maps of $|Z_{in}/Z_0|$ values of R_0

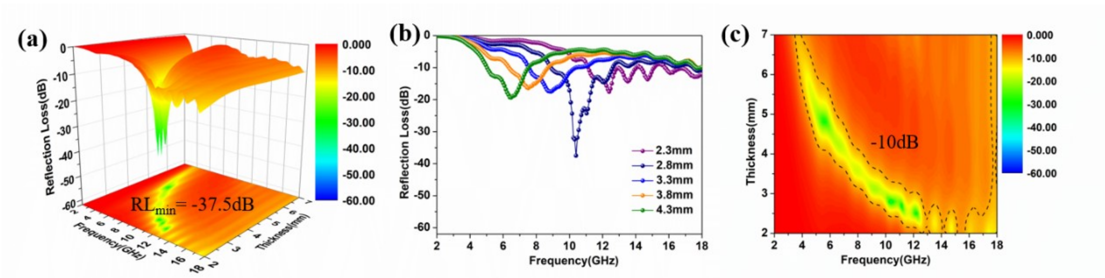

Fig. S10. (a) 3D RL projection mappings, (b) RL curves with different thickness and (c) 2D RL contour maps of R_4 under 5 wt.% loading.

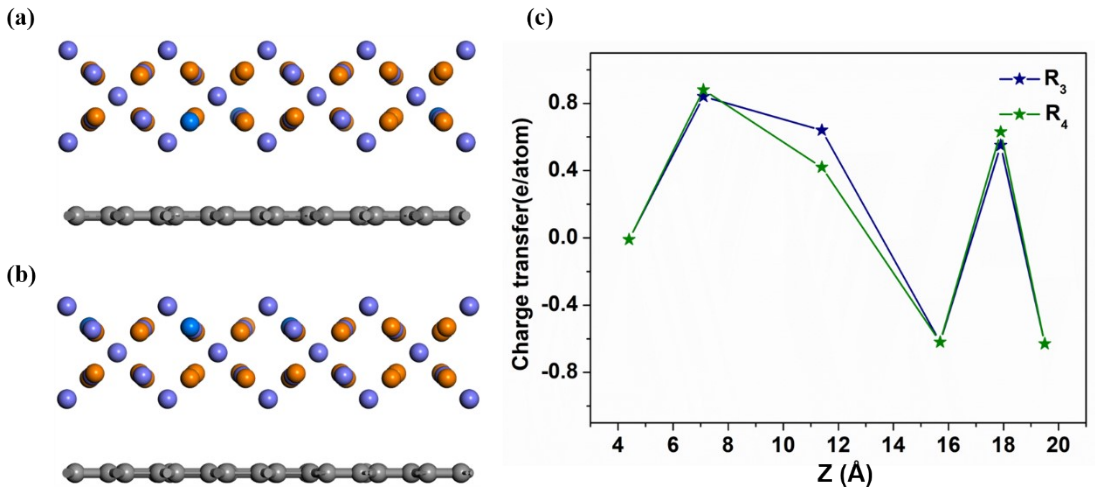

Fig. S11. The crystal structure models of (a) R_3 and (b) R_4. (c) Charge transfer indicated by variation of charge in each atomic layer along the z direction for R_3 and R_4 systems.

The pore size and surface area are obtained by the N_2 adsorption-desorption isotherms and pore diameters of the synthesized composites. As seen in Fig. S12, Co_3O_4 and S-Co_3O_4@RGO aerogels display type IV isotherm with an obvious hysteresis loop in the P/P_0 range of 0-1.0, which indicates the presence of mesopores. Besides, the Barrett–Joyner–Halenda (BJH) pore size distribution analysis (the inset in Fig. S12) reveals that the average pore diameter of Co_3O_4 is mainly concentrated in 2.4 nm and 14.64 nm, and the dominant pore size of S-Co_3O_4@RGO focuses on 2.1 nm. Benefiting from the high porosity, the mesoporous structure and high specific surface area, the 3D aerogel structure improves the reflection of EMW inside the material, and the air entering the pores can modulate the effective permittivity and impedance matching according to the Maxwell-Garnett model[1, 2].

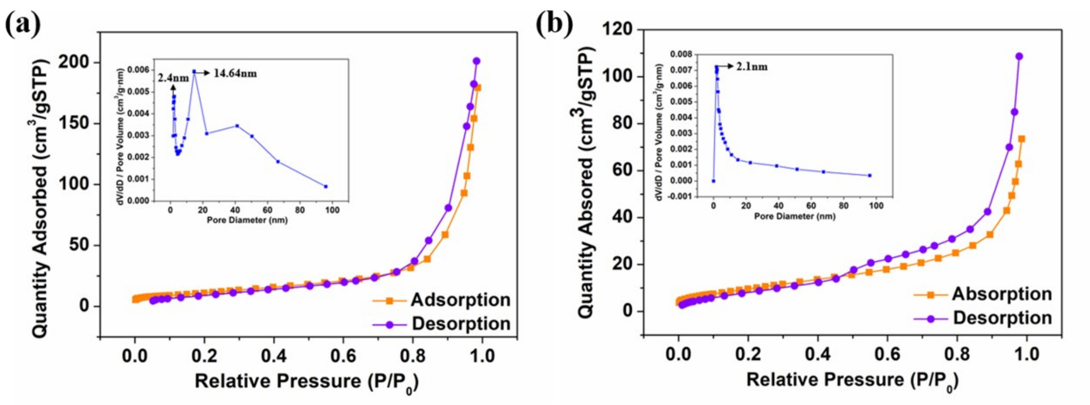

Fig. S12. N_2 adsorption (orange)-desorption (purple) isotherms with corresponding pore-size distributions in the inset for (a) Co_3O_4 and (b) S-Co_3O_4@RGO composites.

To explore the influence of filler loading ratios on the EMW absorption properties, we perform the electromagnetic measurements of the sample of S-Co_3O_4@RGO with three different filler loading ratios.[3] As shown in the figure below, it can be found that the values of RL_{min} of S-Co_3O_4@RGO are −13.1 dB, −56.7 dB and −39.2 dB for the filler loading ratios of 2 wt%, 5 wt% and 8 wt%, respectively. Consequently, the S-Co_3O_4@RGO exhibits the optimal EMW absorption performance with the filler loading ratio of 5 wt%.

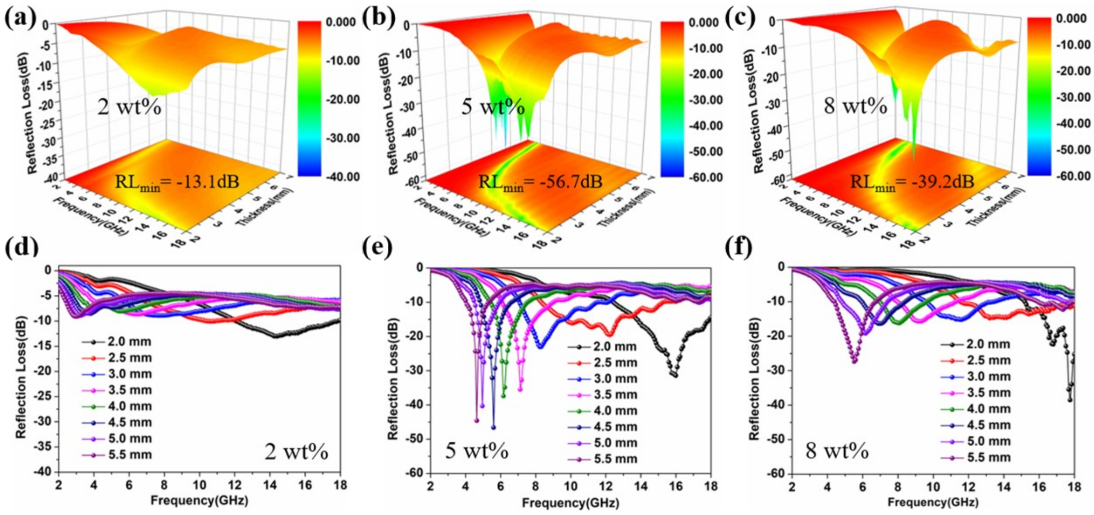

Fig. S12. 3D RL projection mappings of S-Co_3O_4@RGO with filling ratio of (a) 2 wt.%, (b) 5 wt.% and (c) 8 wt.%, RL curves with different thickness of S-Co_3O_4@RGO with filling ratio of (d) 2 wt.%, (e) 5 wt.% and (f) 8 wt.%.

Table S1. Typical EMW absorbers reported in recent literatures.

Samples	Ratios (wt.%)	d (mm)	f (GHz)	RL_{min} (dB)	Bandwidth (GHz)	Ref.
Fe_3O_4/CNTs	30	3	7.12	-35.9	4.3	[4]
FeNi/RGO	20	3	11.12	-39.86	4	[5]
$FeNi_3$@RGO/MoS_2	40	2	14.72	-30.39	4.72	[6]
Co_3O_4 Nanosheets/RGO	5	3.6	5.61	-45.15	5.61	[7]
Co_3O_4/Ni Foam	40	2.1	11.2	-41.1	3.46	[8]
PEDOT/RGO/Co_3O_4	50	2	10.7	-51.1	3.1	[9]
Co/C	40	4	5.8	-35.3	5.8	[10]
Fe_3O_4@SiO_2/RGO	50	1.5	17.8	-26.4	2.6	[11]
Ni/RGO	20	9	13	-24.8	6.9	[12]
$ZnFe_2O_4$/SiO_2/RGO	33	2.8	13.9	-43.9	6	[13]
S-Co_3O_4@RGO aerogels	5	3.6	5.44	-56.7	8.48	This work

Table S2. The binding energy calculation of T_1 and T_2 structures (eV).

Structures	E_{total}	E_1	E_2	E_b
T_1	-102208.43	-10780.75	-15324.80	-76102.88
T_2	-102212.45	-10780.75	-15324.80	-76106.90

The ease of forming a composite structure is characterized by the binding energy, which is defined as: $E_b = E_{total} - E_1 - E_2$, where E_b is the binding energy, E_1 and E_2 represent the energy of different monomers, and E_{total} is the total energy of the composite structure, respectively. The smaller the absolute value of E_b is, the easier the structure is to form.

References

1 X. Qing, X. Yue, B. Wang and Y. Lu, *Journal of Alloys and Compounds*, 2014, **595**, 131-137.

2 F. Pan, Z. Liu, B. Deng, Y. Dong, X. Zhu, C. Huang and W. Lu, *Nanomicro Lett*, 2021, **13**, 43.

3 R. Shu, W. Li, Y. Wu, J. Zhang and G. Zhang, *Chemical Engineering Journal*, 2019, **362**, 513-524.

4 M. Ren, F. Li, B. Wang, J. Wei and Q. Yu, *Journal of Magnetism and Magnetic Materials*, 2020, **513**.

5 A. Dong, Z. Zhiyi, W. Yanhui, C. Shuaishuai and L. Yaqing, *Journal of Superconductivity and Novel Magnetism*, 2018, **32**, 385-392.

6 X. Ding, Y. Huang, S. Li, N. Zhang and J. Wang, *Journal of Alloys and Compounds*, 2016, **689**, 208-217.

7 Y. Ding, Z. Zhang, B. Luo, Q. Liao, S. Liu, Y. Liu and Y. Zhang, *Nano Research*, 2016, **10**, 980-990.

8 W. Gu, B. Quan, X. Liang, W. Liu, G. Ji and Y. Du, *ACS Sustainable Chemistry & Engineering*, 2019, **7**, 5543-5552.

9 P. B. Liu, Y. Huang and X. Sun, *ACS Appl Mater Interfaces*, 2013, **5**, 12355-12360.

10 Y. Lu, Y. Wang, H. Li, Y. Lin, Z. Jiang, Z. Xie, Q. Kuang and L. Zheng, *ACS Appl Mater Interfaces*, 2015, **7**, 13604-13611.

11 Y. Wang, Y. Lai, S. Wang and W. Jiang, *Ceramics International*, 2017, **43**, 1887-1894.

12 Y. Zhang, H. L. Ma, K. Cao, L. Wang, X. Zeng, X. Zhang, L. He, P. Liu, Z. Wang and M. Zhai, *Materials (Basel)*, 2018, **11**.

13 J. Feng, Y. Hou, Y. Wang and L. C. Li, *ACS Applied Materials & Interfaces*, 2017, **9**.